IEEE Access
Multidisciplinary ⋮ Rapid Review ⋮ Open Access Journal

Received 2 May 2023, accepted 17 June 2023, date of publication 27 June 2023, date of current version 5 July 2023.

Digital Object Identifier 10.1109/ACCESS.2023.3289813

RESEARCH ARTICLE

Multi-Objective Optimal Planning of Virtual Synchronous Generators in Microgrids With Integrated Renewable Energy Sources

MD. SHADMAN ABID[1], (Student Member, IEEE), RAZZAQUL AHSHAN[1], (Senior Member, IEEE), RASHID AL-ABRI[1], (Member, IEEE), ABDULLAH AL-BADI[1], (Senior Member, IEEE), AND MOHAMMED ALBADI[1,2], (Senior Member, IEEE)

[1]Department of Electrical and Computer Engineering, College of Engineering, Sultan Qaboos University, Muscat 123, Oman
[2]Arab Open University, Muscat 130, Oman

Corresponding author: Razzaqul Ahshan (razzaqul@squ.edu.om)

This work was supported by the Sustainable Energy Research Center (SERC), Sultan Qaboos University (SQU), under Grant IG/DVC/SERC/22/01.

ABSTRACT Appropriate renewable distributed generation (RDG) placement is one of the most significant issues for the efficient operation of current power systems. Since the inverter-interfaced RDG lacks rotating mass to sustain the system's inertia, microgrids have low total system inertia, which impairs frequency stability and can yield significant frequency and voltage instability in severe disruptions. The virtual synchronous generator (VSG), which uses concepts that regulate the inverter to simulate a conventional synchronous generator, is one of the most promising solutions to address these challenges. Hence, this research proposes a unique technique of simultaneous optimal solution for RDG and VSG sizing and placement in distribution networks using a recent metaheuristic technique called the Multi-objective Salp Swarm Optimization Algorithm (MOSSA). The objective function was to minimize the frequency deviation and maximize the total annual energy savings and operational costs of the RDG and VSG units. This study assesses IEEE 33 bus, 69 bus distribution network, and practical Masirah network as the test systems. Moreover, the MOSSA Pareto fronts are superior to two recent metaheuristics employed in this research domain: Multi-objective Particle Swarm Optimization (MOPSO) and Non-dominated Sorting Genetic Algorithm-II (NSGA-II). The results demonstrate that the MOSSA Pareto fronts satisfied the frequency and energy-saving objectives. In addition, all Pareto fronts accurately prevented voltage limit infringements, and the overall energy losses were significantly reduced.

INDEX TERMS Virtual synchronous generator, optimization, multi-objective algorithm, renewable energy, distributed generation.

NOMENCLATURE

b	Branch index.
i	Bus index.
NBR	Total number of branches
P_{gen}	Actual power generation.
P_{load}	Active demand.
P_{loss}	Active loss.
Q_{gen}	Reactive generation.
Qr_{load}	Reactive demand.
Qr_{loss}	Reactive loss.
S_l	Power transmitted in branch l.
Vm_{bus}	Voltage at a certain bus.
$C_{RDG/VSG}$	Cost per kW of injected power .
$S_{RDG/VSG,m}$	Size of m^{th} RDG/VSG.
$S_{RDG/VSG,max}$	Allowable maximum size .
$T_{RDG/VSG}$	Total RDG/VSG lifetime in years.
C_E	Average cost of energy loss per kWh.
R	Rate of interest on capital investment of the installed RDG-VSG.
$AEL_{T,RDG/VSG}$	Total annual economic loss with RDG/VSG.

The associate editor coordinating the review of this manuscript and approving it for publication was Rajesh Kumar.

$AEL_{T,noRDG/VSG}$	Total annual economic loss without RDG/VSG.
CRF	Capital recovery factor.
$P_{RDG/VSG,m}$	Active power output of m^{th} RDG/VSG.
P_{loss}	Total active power loss.
$P_{loss,b}$, $Q_{loss,b}$	Active and reactive power loss of bus b.
$P_{loss,no-RDG/VSG}$	Total active power loss without integrating RDGs and VSGs.
$P_{loss,RDG/VSG}$	Total active power loss after integrating RDGs and VSGs.
$TAES$	Total annual energy saving.

I. INTRODUCTION

Due to the rising adoption of renewable energy sources (RES), the energy distribution architecture is gradually transitioning from consolidated conventional power generation to distributed energy production. Recent years have seen a significant increase in integrating distributed power production units based on RES [1], [2]. The optimum utilization of renewable energy sources is facilitated by digitally controlled power electric converters or inverters that enhance the power systems' flexibility by offering a swift transient performance. In contrast to conventional power generating units, where synchronous generators (SG) use their rotational momentum to offer frequency support during disturbances, renewable systems can assist in frequency support by contributing virtual inertia via electronic inverters [3]. Nevertheless, RDGs electronically connected to the grid or power systems exhibit different traits from traditional power-producing units. Electronic inverters control the power generated at interfaced RDGs; however, they cannot provide the necessary inertia and damping to the power grid. Inverter-based distributed generation is often controlled via grid-connected current control. However, this approach has a variety of drawbacks, including the inability to operate independently and frequency instability that inhibits the expansion of RES penetration [4]. The solution to this challenge, however, is devised by applying appropriate control techniques to the grid-connected inverter and managing its switching pattern such that it operates as an SG by replicating the behavior of a conventional SG. In this context, VSGs are introduced, known as grid-connected inverters that imitate the steady-state and transient properties of SG [5], [6], [7]. VSG-integrated systems are expected to represent the future of power system networks. Therefore, it is critical to analyze and enhance the transient stability of VSG-based power systems.

Numerous studies have been conducted in recent years to investigate the potential benefits and drawbacks of VSG implementation on microgrids. For example, the droop control [8] approach was developed to modulate real and reactive power using a paradigm comparable to the parallel operation of synchronous machines; however, it was unable to completely address the problems of low inertia and frequency stability of microgrids. The virtual synchronous generator (VSG), which uses concepts that regulate the inverter to simulate a conventional SG, is one of the most promising solutions in this research domain [9]. A thorough explanation of the VSG structure was offered in the works of [10], along with an overview of several topologies for virtual inertia and VSG control, including active power allocation, reactive power allocation, voltage control, and frequency regulation. The issues with VSG and potential avenues for future study were also explored, including centralized control, stability improvement, and interfacing for VSG.

Furthermore, several studies have used optimization techniques to investigate the potential benefits and restrictions of implementing VSG on electrical grids. For example, in the works of [11], the dynamic stability of several grid-connected voltage source converters controlled by VSG was investigated with active power control. Besides, the design approaches for a multi-VSG damping controller based on a hybrid particle swarm optimization technique and residue index were considered. Numerous simulations and test cases of the multi-VSG grid-connected system were conducted to demonstrate the efficiency of the damping controller design method. Furthermore, in [12], the authors proposed a self-adaptive VSG active power control strategy using fuzzy logic-based genetic algorithms to create specific fuzzy rules with the allocation of distributed generation units and frequency deviation as input parameters. The results show minimal frequency deviation based on constant inertia parameters. Besides, the study in [13] used two objective function functions to create an ideal VSG active power control scheme using particle swarm optimization (PSO). The first objective was to minimize the integral time absolute error, and the second objective considered the frequency deviation of the grid. In the works of [14], PSO is used to investigate how VSG affects reducing voltage drop and power fluctuations and restricting the maximum fault current of distribution lines. Moreover, in the works of [15], a novel trustworthy metaheuristic optimization method known as the artificial hummingbird algorithm (AHA) is used to fine-tune the parameters of the proposed VSG controller by constructing the load frequency control based on a two-area linked power system, the suggested AHA is superior to other potent optimization strategies as the marine predators' algorithm, grey wolf optimizer, and artificial bee colony optimization. Moreover, in the works of [16], the authors utilized a proportional-integral (PI) controller that had been ideally built using the manta ray foraging optimization algorithm as the foundation for controlling the virtual inertia control loop. The effectiveness of the MRFO-based PI controller was examined in light of various operating situations and contrasted with that of conventional PI controllers based on evolutionary optimization algorithms. Moreover, by improving the settings of the virtual inertia controller while taking into account VSG dynamics and the uncertainties of system inertia, a whale optimization technique is utilized to improve the virtual inertia control loop [17]. Furthermore, to fine-tune the settings of the aforementioned

VSG controller, a unique sine augmented scaled arithmetic optimization approach is suggested in the works of [18]. Using simulation results, the usefulness of the suggested technique is verified, and the effects of a few common tactics, such as a change in system boundaries and different stages of RESs penetration, are also demonstrated. Likewise, the authors of the work [19] developed the combined whale and the ant lion algorithm. The study aimed to improve the grid voltage and frequency affected by the variations of inertia.

Moreover, achieving the global minimum of an RDG placement and sizing function is much more complex, and numerical solution methodologies often allude to substantial problems; the researchers employed a variety of multi-objective frameworks. For example, a multi-objective optimization approach was created by the authors of the study [20] in order to maximize the use of RESs while minimizing the cost of energy and the likelihood of an energy supply breakdown. Moreover, MOPSO was utilized for three different energy system designs in works of [21] with the objectives of cost minimization and voltage stability maximization. Furthermore, a multi-objective algorithm was created in the works of [22] to determine the optimal placement of RDG units for Turkey by considering financial, environmental, and technical characteristics. Besides, the study cited in [23] investigated the size and position of wind turbine (WT) and photovoltaic (PV) units in distribution networks using chaotic sequence spotted the hyena optimizer technique to reduce loss and improve the voltage profile and stability index. Furthermore, the study in [24] proposed a novel metaheuristic approach employing the AHA technique to find the proper locations and sizes of biomass-based RDGs in radial distribution networks by reducing the switching frequency and total system energy loss. Besides, the authors of the paper [25] presented symbiotic microorganism exploration algorithm for RDG placement in microgrids for different test systems. Moreover, the work in [26] guaranteed the homogeneity of the Pareto fronts and advocated an improved NSGA II. Furthermore, the work in [27] suggests a multi-objective equilibrium optimizer-based technique that includes several objectives, including reducing the operation and investment costs, energy pricing, power loss penalties, and carbon emissions penalties for the integrated units.

The researchers have contributed by developing the multi-objective model for the ideal size, placement, and type of RDG units utilizing various heuristic or stochastic methods. However, the solutions found cannot be guaranteed to be globally optimum. For example, to maximize the real power loss and the yearly expenses of system components, the multi-objective slime mould algorithm was utilized in [28]. Similarly, the work in [29] suggested a unique chaos pupil sociology and anthropology optimization algorithm for locating RDG units considering the stochastic generation pattern. Furthermore, to upgrade the RDG-based storage systems, the authors of [30] employed a thorough evaluation of RDGs using a linear modeled optimization algorithm. Additionally, to expand the penetration of RDG systems, the study's authors created a hybrid system model based on a grid-connected discrete harmony search algorithm [31]. Similarly, the research in [32] offered a multi-temporal optimal power flow approach that guaranteed accurate and optimal solutions with higher performance utilizing the convex power flow method. Moreover, the study in [33] suggested a combination model using a binary programming-based optimization approach to enhance RDG penetration. Likewise, the study in [34] developed the multi-objective multi-verse approach for the RDG allocation challenge in microgrids to enhance voltage profiles and reduce yearly expenses. Furthermore, in [35], optimal allocation issues of RDGs were resolved using a meta-heuristic algorithm coupled with a stochastic model known as monte carlo simulation. Besides, a planning strategy for the best RDG size and control was developed in [36] to reduce the curtailment from RDGs. Additionally, to estimate the ideal size of RDGs for a residential house, the authors of [37] suggested a stochastic optimization problem using mixed-integer linear programming. Moreover, [38] examined the ideal sizing and positioning of RDGs for an area in Jordan by performing a feasibility analysis utilizing the HOMER software program.

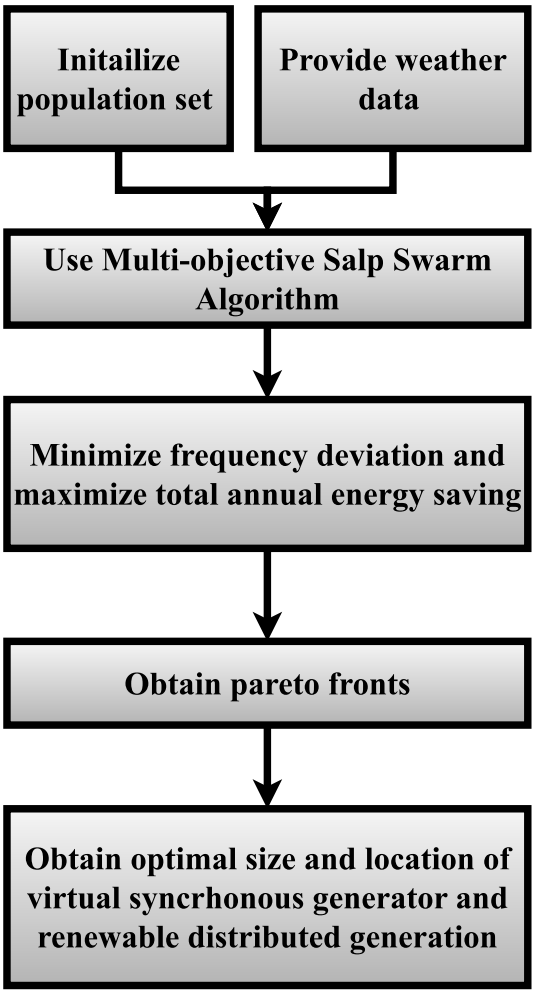

FIGURE 1. Proposed framework.

A. MOTIVATION

The literature review and current research initiatives highlight the necessity for additional attention to formulating and resolving problems related to the optimum RDG and VSG integration into different distribution systems. The previous researches show that the set value of the active power output from the VSG is a crucial consideration when implementing VSG. In order to restore the frequency of microgrids to the permitted limits, the quantity of active power allocated during regular operation needs to be carefully controlled. Additionally, incorporating RDG units in microgrids necessitates extensive planning and design to meet the electric network's performance criteria, such as voltage stability, power quality, total active power loss reduction, and economic efficiency. Moreover, numerous metaheuristic algorithms have been utilized in prior studies to address these issues, but none of the techniques guarantees the optimal global solution. The research gaps from the literature review section are identified below:

- Prior research mostly overlooked the simultaneous optimum implementation and design of VSG units with various RDG types.
- Including several objectives in optimization increases the challenge and needs decision support.
- No preceding study can vouch for the techniques' global superiority.
- Heuristic approaches are desirable for solving non-linear optimization problems when there are a variety of control variables. This study area exhibits multi-objective scenarios with unknown Pareto optimum solutions and needs to be investigated by recent heuristic algorithms.
- The recommended methodologies' techno-economic assessment in various distribution systems was primarily neglected in earlier studies.

B. MAIN CONTRIBUTIONS

To address the research gaps, this research suggests a novel method for identifying Pareto solutions for simultaneous RDG and VSG unit placement and sizing. Moreover, the proposed framework of this study is depicted in Fig. 1. The main contributions of this research work are identified as follows:

- To improve microgrids' voltage and frequency stability, the conventional RDG allocation problem is combined with VSG's optimal active power distribution.
- The Multi-objective Salp Swarm Optimization Algorithm (MOSSA) [39], a recently developed technique, is used to identify the solution with the greatest exploitative aspect and exploration competency.
- MOSSA is compared with two contemporary multi-objective algorithms: MOPSO [21] and NSGA-II [26].
- IEEE 33 bus, 69 bus, and practical Masirah distribution network are examined.
- Oman's meteorological information is incorporated in the RDG and VSG placement simulation.

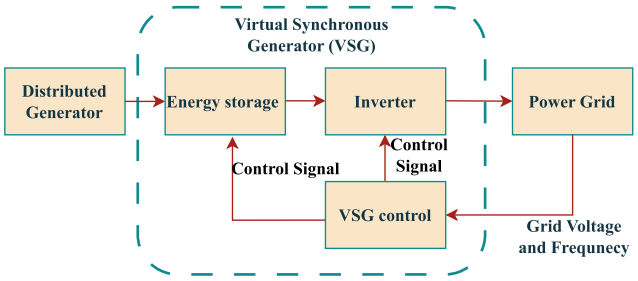

FIGURE 2. VSG block diagram.

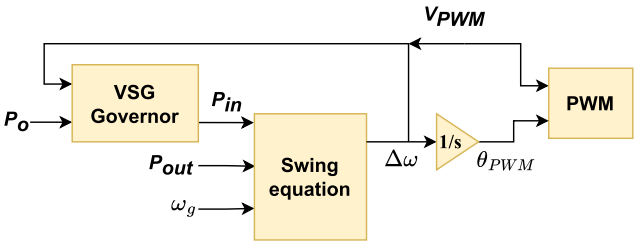

FIGURE 3. Virtual inertia control diagram.

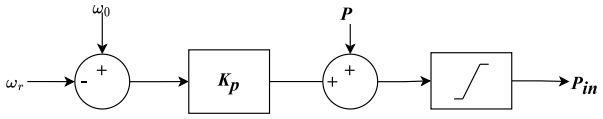

FIGURE 4. VSG governor diagram.

- Frequency deviation minimization and total annual energy saving minimization are considered as the objectives.

II. VIRTUAL SYNCHRONOUS GENERATORS

As demonstrated in Fig.2 VSG comprises three essential components - inverter, energy storage, and a virtual inertia control mechanism. An inverter controlled by the VSG concept connects a distributed resource to the primary power grid. Moreover, virtual inertia control, another crucial component of VSG, represents the SG's swing equation as expressed in Eq.1 [10].

$$P - P_{out} = 2H\frac{\mathrm{d}\Delta\omega_r}{\mathrm{d}t} + K_d\Delta\omega_r \tag{1}$$

here, P denotes VSG input power per unit, P_{out} represents measured grid power output, H is the virtual inertia constant. The virtual angular rotor speed (ω_r) per unit can expressed as Eq. 2:

$$\Delta\omega_r = \omega_r - \omega_g \tag{2}$$

where ω_g is the per-unit angular rotor speed of the measuring point, and K_d represents the VSG's virtual damping coefficient per unit. Fig.3 demonstrates the control diagram of VSGs. Moreover, the VSG Governor represented in Fig.4 is an $\omega - P$ droop controller. Furthermore, ω_0 represents the system's nominal angular frequency, P denotes the active power set value, K_p means the droop coefficient per unit equal to $1/\delta$, and δ represents the speed regulation factor.

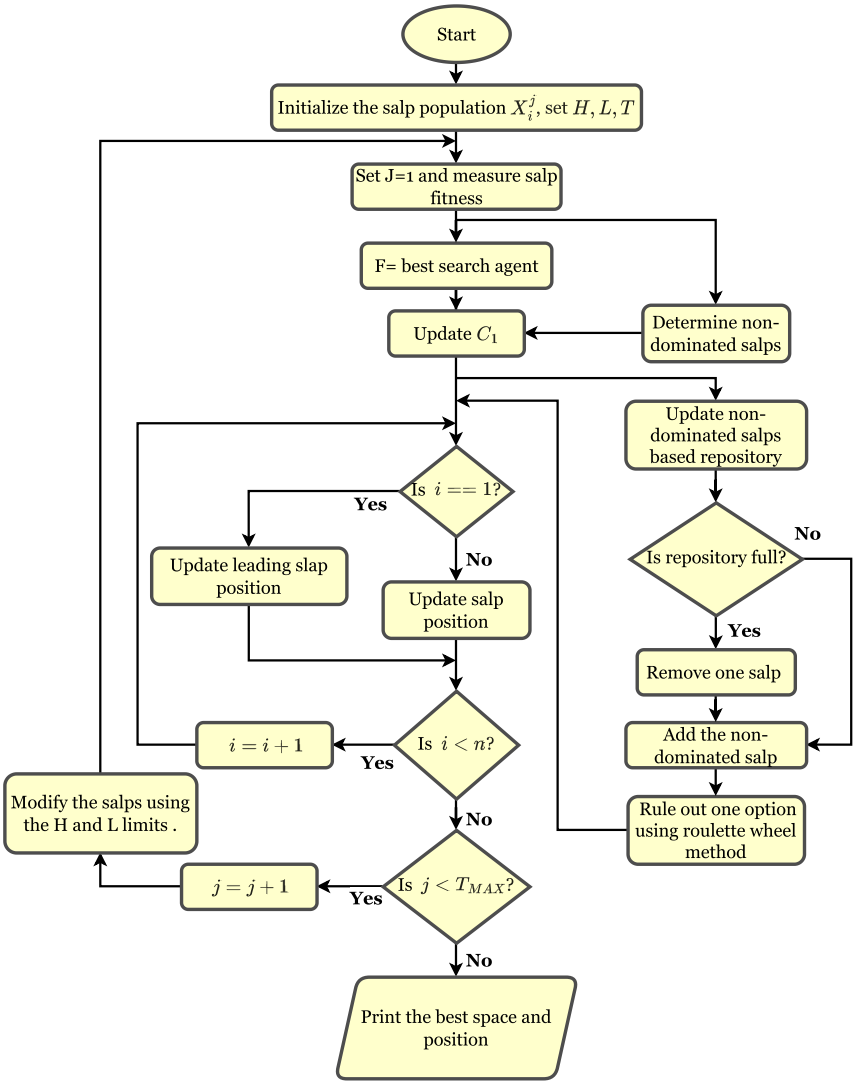

FIGURE 5. MOSSA flowchart.

III. MULTI-OBJECTIVE SALP SWARM OPTIMIZATION ALGORITHM (MOSSA)

In order to achieve rapid convergence and accomplish high variation while coordinating many objectives, MOSSA focuses on a set of solutions. It takes its cues from the swarm behavior of salps in seas and employs the salp chain for the exploration and extraction processes. Fig.5 illustrates the stages of the MOSSA approach. The salp chain is composed of the leader and followers. The first chain's leader points the blooms differently, and the others obediently imitate. MOSSA describes the salps position as a search space whose dimension relies on the number of variables. To preserve the orientation, 2-dimensional matrices are employed. The leader position and food supply are changed with each optimization cycle. The steps of the leader's position are expressed in Eq. 3:

$$X_j^1 = \begin{cases} F_j + C_1((H-L)C2 + L) & C_3 \geq 0.5 \\ F_j - ((H-L)C2 + L) & C_3 < 0.5 \end{cases} \quad (3)$$

Here, X_j^1 denotes the position of the leader, F_j represents the position of the food source F in j dimension, H and L means the maximum and minimum Bounds, C_2 and C_3 are random numbers between 0 and 1. The following equation describes C_1, which is crucial during the exploration and exploitation phases.

$$C_1 = 2e^{-\left(\frac{4T}{T_{MAX}}\right)^2} \quad (4)$$

Here, T is the current iteration, and the maximum number of iterations is T_{MAX}.

A. PENALTY-BASED BOUNDARY INTERSECTION (PBI)

The PBI method is used to scalarize two nonlinear dimensional objectives in conflict. This can be stated as:

$$g^{PBI}(X|W,\theta) = d_1 + \theta d_2$$
$$d_1 = \frac{\left\|(f(X) - z^*)^T W\right\|}{\|W\|}$$

$$d_2 = \left\| f(X) - (d_1 \frac{W}{\|W\|} + z^*) \right\| \quad (5)$$

here, θ means penalty parameter of ($\theta \geq 0$), W denotes direction vector and z^* represents the optimal point.

B. NON-SCALE APPROACH (NS)

Non-scale approach converts the two competing objectives into a mono-objective function by weighting and aggregating them and can be expressed as:

$$OF_i(X) = \frac{OF_i(X) - OF_i^{Min}(X)}{OF_i^{Max}(X) - OF_i^{Min}(X)} \quad (6)$$

here, $OF_i^{Max}(X)$ and $OF_i^{Min}(X)$ represents the upper and lower boundaries of i individual objective function and W_i denotes the weight coefficients ($0 > W_i < 1$).

C. NON-DOMINATED ROULETTE WHEEL METHOD

A distinct case arises when one identical non-dominated solution of the repository's inhabitants is discarded in contrast to the solutions in the repository, and the salp is not dominant. Using a roulette wheel, the solution is to identify non-dominated solutions utilizing the populous neighborhood by counting the number of neighborhood solutions with the greatest distance. The distance vector expressed in Eq. 7 is expressed as:

$$D = \frac{\overrightarrow{MAX} - \overrightarrow{MIN}}{Repository\ size} \quad (7)$$

IV. SIMULATION MODELING

In order to ensure that the system can survive in the case of a substantial interruption that isolates the microgrid from the utility grid, MOSSA is utilized in this study to distribute active power output from VSG and apparent power from RDG units. The fitness function used in this study aims to determine the appropriate location and size of RDGs and VSGs to minimize total frequency deviation and annual energy-saving cost while complying with the constraints mentioned in [40].

$$objective\ function = minimize\ \Delta f \quad while\ maximizing\ TAES \quad (8)$$

where,

$$TAES = AEL_{T,no\ RDG/VSG} - AEL_{T,RDG/VSG} \quad (9)$$

$$AEL_{T,noRDG/VSG} = P_{loss,no-RDG/VSG} * C_E * 8760 \quad (10)$$

$$AEL_{T,RDG/VSG} = P_{loss,RDG/VSG} * C_E * 8760 + [(C_{RDG/VSG} * \sum_{m=1}^{N_{RDG/VSG}} P_{RDG/VSG,m})/CRF] \quad (11)$$

$$CRF = [R * (1+R)^{T_{RDG/VSG}}] / [(1+R)^{T_{RDG/VSG}} - 1] \quad (12)$$

TABLE 1. Input parameters for RDG and sizing and placement.

Parameter	Value
$C_{RDG/VSG}$ ($/kW$) [40]	30
$T_{RDG/VSG}$	10
C_E ($/kWh$)	0.05
$R(\%)$	10

TABLE 2. Test systems.

Stat	IEEE 33 bus	IEEE 69 bus	Masirah network
$P_{loss,no-RDG/VSG}$ (kW)	202.5	220.3	301.24
Frequency deviation (p.u)	0.0934	0.0834	0.4047
ROCOF (50% RDG penetration)	0.0185	0.0190	0.0540

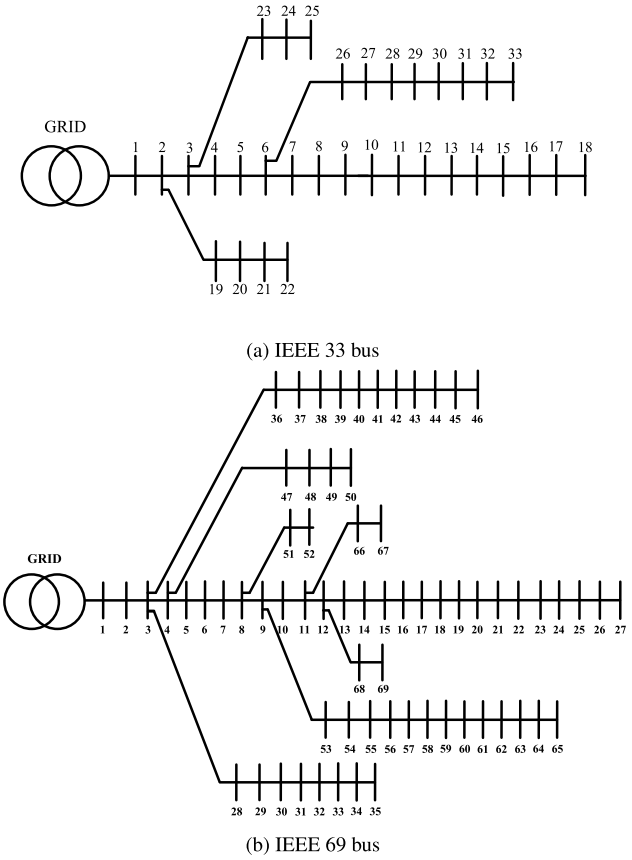

FIGURE 6. Single line diagram.

In this study, a fixed RDG was installed in the test systems shaping it into a microgrid to examine the frequency deviation value before and after optimization. The utility grid was then disconnected from the grid in order to operate in islanded mode with only one RDG. Following this, the optimization problem was solved to determine the optimal VSG and RDG unit placement.

A. OPERATIONAL CONSTRAINTS

Certain operational constraints should be considered during the optimization procedure, which are demonstrated below:

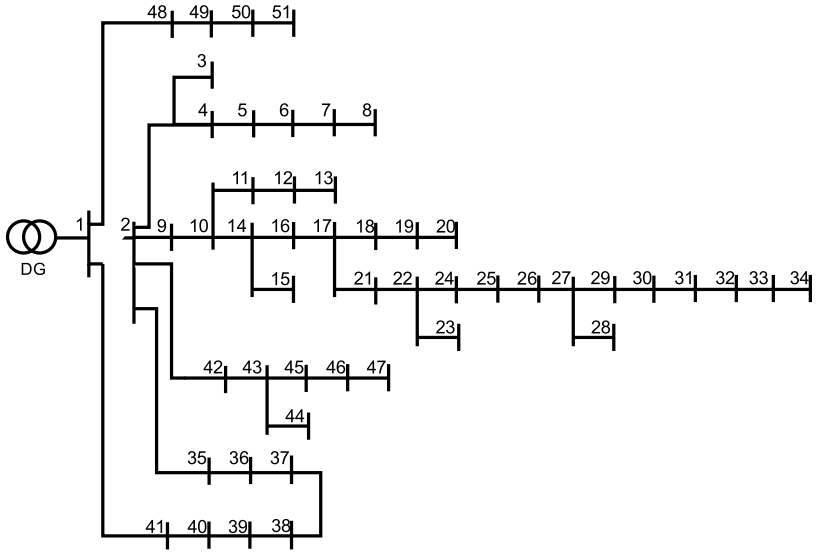

FIGURE 7. Single line diagram of Masirah Island.

i. **Power balance**: The total electricity production must equal the sum of the total losses, as well as the load demand.

$$\sum P_{gen} = \sum_{i=1}^{i} P_{load} + \sum_{b=1}^{NBR} P_{loss} \tag{13}$$

$$\sum Q_{gen} = \sum_{i=1}^{i} Qr_{load} + \sum_{b=1}^{NBR} Qr_{loss} \tag{14}$$

ii. **Voltage constraint**: Voltage levels on each bus (Vm_{bus}) are restricted to a suitable range.

$$0.9\ p.u \leq Vm_{bus} \leq 1.1\ p.u \tag{15}$$

iii. **Branch loading**: The apparent load transmitted in branch l should not exceed the branch's thermal limit.

$$S_l \leq S_{l-max} \tag{16}$$

v. **RDG and VSG Capacity Constraints**: In this study, the minimum ($P^{min}_{RDG}, Q^{min}_{RDG}$) and maximum rating ($P^{max}_{RDG}, Q^{max}_{RDG}$) of RDG has been considered as 0.1 MVA to 2.3 MVA with a constant power factor of 0.9 per unit (p.u). Furthermore, the minimum (P^{min}_{VSG}) and maximum (P^{max}_{VSG}) rating of VSG is considered as 0.1 MW and 6 MW [24].

$$P^{min}_{RDG} \leq P_{RDG} \leq P^{max}_{RDG} \tag{17}$$

$$Q^{min}_{RDG} \leq Q_{RDG} \leq Q^{max}_{RDG} \tag{18}$$

$$P^{min}_{VSG} \leq P_{VSG} \leq P^{max}_{VSG} \tag{19}$$

B. SIMULATION PROCEDURE

The following procedure outlines the structure of the proposed MOSSA algorithm for determining ideal VSG and RDG locations and sizes, as well as their operating methods:

Step 1: Supply the initial parameters that include the maximum quantity of RDGs and VSGs, size and positional constraints, population size, RDG and VSG modeling, and the load demand curve.

TABLE 3. MOSSA results for IEEE 33 bus in 72 hour optimization period.

Parameter	Results
PV size (MVA)	0.80
WT size (MVA)	0.99
VSG size (MW)	2.08
PV location	29
WT location	15
VSG location	5
Frequency deviation (p.u)	0.000056
ROCOF(Hz/s)	0.0916
H (MJ/MVA)	8.9241
TAES (USD)	65988.06
Power Losses (MWh)	3.79

Step 2: Create the initial population set based on algorithmic factors such as population size (40). A vector composed of the positions and capacities of VSG and RDG units is employed to demonstrate a population.

Step 3: Population variable ranges are randomly dispersed within bounds, as the RDG locations, types, sizes, and VSG operation technique.

Step 4: Conduct load flow calculations for each population.

Step 5: Employing the MOSSA exploitation approach, formulate the locations to reflect the favored candidate. (Subsection III)

Step 6: Check if the solutions fall within the parameters specified in Subsection. IV-A.

Step 7: *Steps* 5 and 6 should be repeated until the permitted number of repetitions is achieved. The stopping threshold for all algorithms in this study was set at 20 iterations.

Step 8: Provide the Pareto solution.

C. TEST SYSTEMS AND DATA

The ROCOF, frequency deviation, and the power losses for the test systems without RDG and VSG placement are depicted in Table 2. To find out the ROCOF mentioned

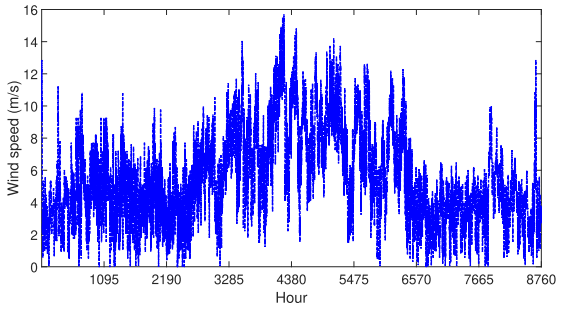

(a) Wind velocity

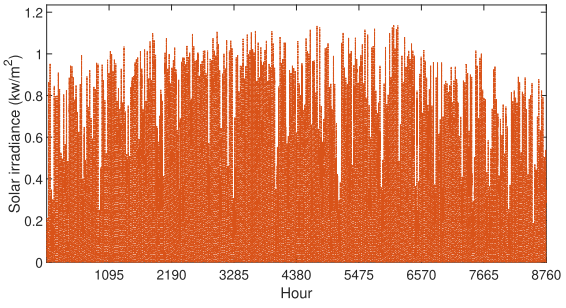

(b) Solar irradiance

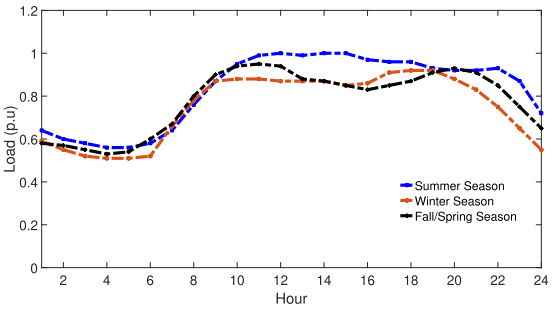

(c) Load demand

FIGURE 8. Weather and load data for Masirah network.

in Table 2, an RDG with 50% of the total generation was attached to the grids at random locations on the base case islanded networks. The IEEE 33 bus test system [42], 69 bus system [43], and Masirah network [44] are assessed in this study (Fig. 6 and Fig. 7). Furthermore, Masirah Island's solar radiation and wind speed are obtained from [45] and [46]. To accommodate for weather-related variability in the load and RDG outputs, a simulation time of 72 hours (3 typical days for each season with average hourly outputs) was adopted. The one-year wind, solar, and load data are depicted in Fig. 8.

V. RESULTS ANALYSIS

Using the suggested MOSSA applied to the aforementioned test systems (IEEE 33, IEEE 69, and Masirah Island), the following simulated cases are taken into consideration. Moreover, the obtained results by the MOSSA are compared with the other algorithms, such as MOPSO and NSGA-II.

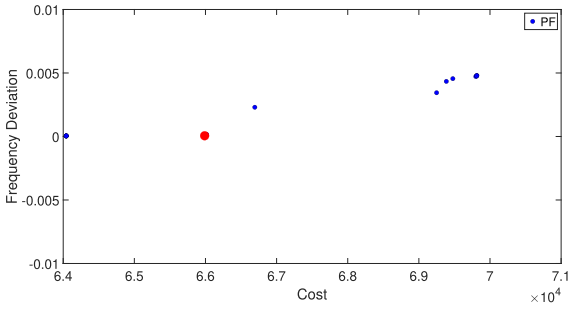

FIGURE 9. MOSSA PSC for 33-bus.

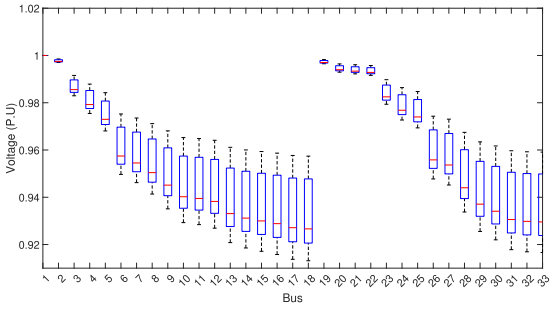

(a) Base Case

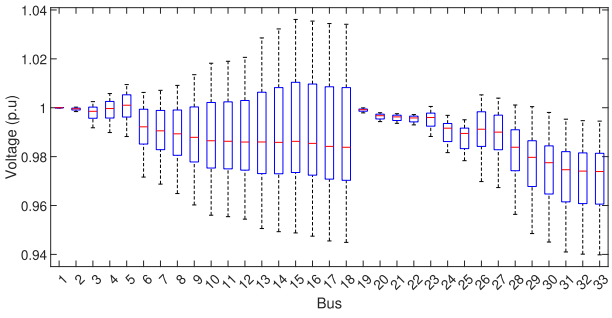

(b) MOSSA PSC

FIGURE 10. Voltage profile for 33-bus.

A. SIMULTANEOUS RDG AND VSG PLACEMENT

The following sections demonstrate the results obtained for the case of simultaneous VSG and RDG placement case for the three test systems using MOSSA based technique:

1) RESULTS FOR IEEE 33 BUS

Fig. 9 shows the Pareto solution candidates (PSCs) of the MOSSA method. The vertical axis shows the frequency, and the horizontal axis illustrates the yearly energy-saving costs of RDG and VSG units. The non-dominated solutions produced after 20 optimizations are referred to as PSCs. The decision-making procedure selects the best Pareto-front choices. This method is based on selecting the solution with the least slope and no voltage magnitude violations [41]. This optimum Pareto solution candidate's objective function values are Δf = 0.000056 and *TAES* = 65988.06 USD. The capacity and the locations of RDGs and VSGs for the PSC are displayed in Table 3. As the islanded microgrid has the optimal RDG size and placement paired with active power allocation from VSG at the suitable location, the frequency

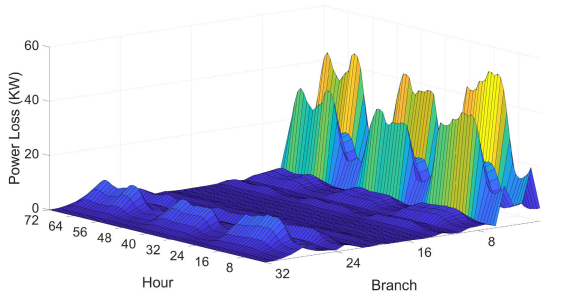

(a) Base Case

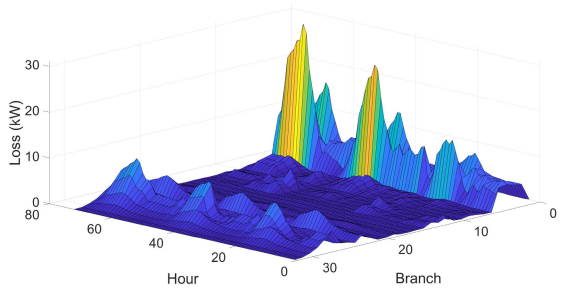

(b) MOSSA PSC

FIGURE 11. Loss profile for 33-bus.

TABLE 4. MOSSA results for IEEE 69 bus in 72 hour optimization period.

Parameter	Results
PV size (MVA)	1.07
WT size (MVA)	0.75
VSG size (MW)	2.16
PV location	54
WT location	31
VSG location	8
Frequency deviation (p.u)	0.000066
ROCOF(Hz/s)	0.0934
H (MJ/MVA)	8.788
TAES	26213.06
Power Losses (MWh)	6.707

deviation value is decreased by 99.7% for the IEEE 33 test systems. Furthermore, the VSG provides 8.9241 MJ/MVA inertia to the grid. The results also reveal that MOSSA's PSCs decrease test system variance in voltage and provide an adequate trade-off between the objectives. Furthermore, a comparison of the network voltage profile before and after the simulation is shown in Fig. 10. The findings show that a minimum voltage of 0.9134 pu at bus 18, during the summer, at 5 p.m., was increased to 0.944 pu. Additionally, Fig. 11 shows how real power losses have decreased for each branch and hour compared to base case scenarios. The voltage profile adjustments additionally resulted in a decreased active power loss value. Compared to the base scenario, the PSC decreases total energy losses by 53.2% (8.1 MWh to 3.79 MWh). Moreover, the results suggest substantial loss reductions are achieved during the peak load hours, which makes the network more efficient in terms of power quality.

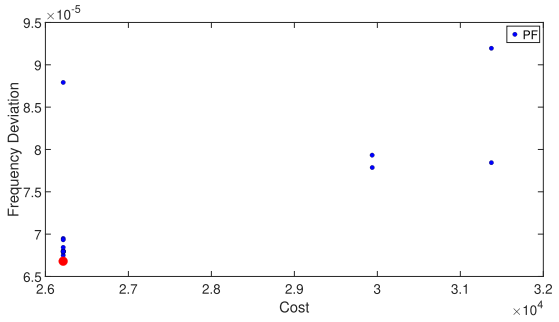

FIGURE 12. MOSSA PSC for 69-bus.

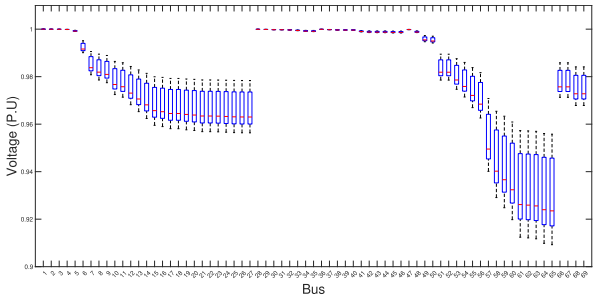

(a) Base Case

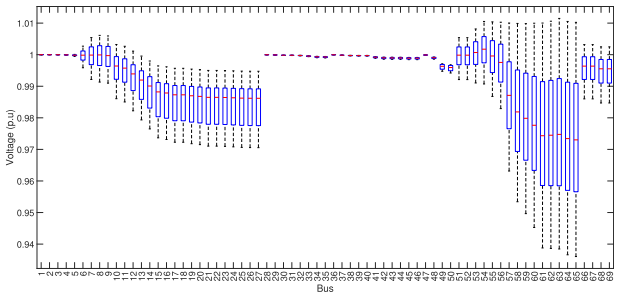

(b) MOSSA PSC

FIGURE 13. Voltage profile for 69 bus.

2) RESULTS FOR IEEE 69 BUS

Fig. 12 depicts the Pareto fronts obtained by the MOSSA method for 69 bus system. The objective values are Δf = 0.000066 and *TAES* = 26213.06 USD. The approaching RDG and VSG capacity and location for the Pareto front are illustrated in Table 4. The frequency deviation value is reduced by 99.7% for the IEEE 69 bus test systems because the islanded microgrid has the ideal RDG size and placement and active power allocation from VSG at the appropriate location. Fig. 13 depicts the voltage profile contrasts for the PSC and base case. The minimum voltage magnitude rises from 0.9102 pu in the base case to 0.927 pu in the PSC. Furthermore, Fig. 14 depicts the reductions in PSC branch real power losses. Moreover, the VSG provides 8.788 MJ/MVA inertia to the grid. It should be emphasized that power losses during peak hours are decreased by 533.33, 19.79, and 275.98% for the summer, spring, and winter seasons, respectively. Total energy losses for PSC are 6.7 MWh, compared to 11.5 MWh under base case conditions.

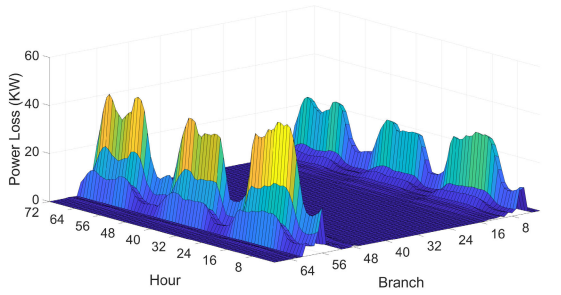

(a) Base Case

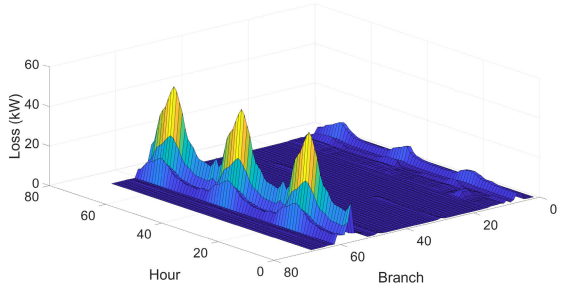

(b) MOSSA PSC

FIGURE 14. Loss profile for 69 bus.

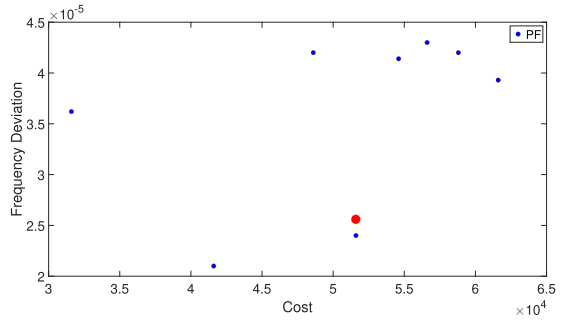

FIGURE 15. MOSSA PSC for Masirah network.

3) RESULTS FOR MASIRAH NETWORK

Fig. 13 depicts the Pareto fronts obtained by the MOSSA method for Masirah network. The objective values for the PSC are $\Delta f = 0.000025$ and $TAES = 51590.21$ USD. Table 5 depicts the RDG and VSG locations and capacity obtained by MOSSA. Fig. 16 compares the node voltage profiles before and after optimization. The findings show that the minimum voltage value for base case circumstances is 0.928 pu, whereas the minimum voltage value for PSC is 0.939 pu. The Masirah Island test systems had a 99.9% decrease in frequency deviation due to inertia support (9.351 MJ/MVA) and active power allocation from VSG at an appropriate location. Furthermore, Fig. 17 shows the real power loss values for the branches. The overall energy losses for PSC are 7.6 MWh, compared to 13.7 MWh in the base case scenario.

B. ONLY VSG PLACEMENT

Table 6 displays the MOSSA results for only VSG placement. In this case, a single distributed generating unit linked to the slack bus and feeding the whole network supplies the

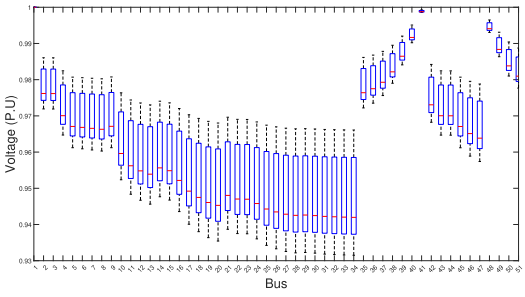

(a) Base Case

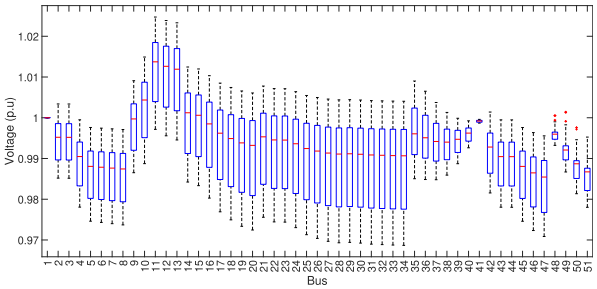

(b) MOSSA PSC

FIGURE 16. Voltage profile for Masirah network.

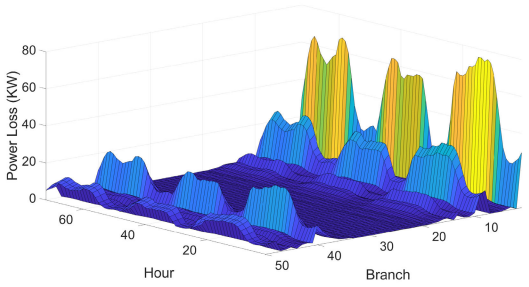

(a) Base Case

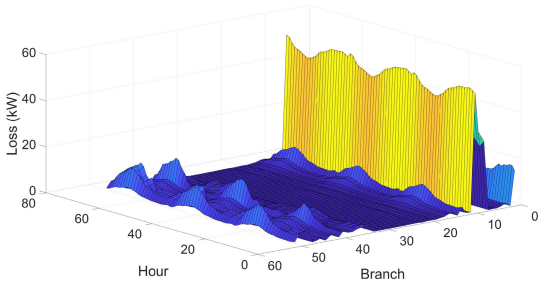

(b) MOSSA PSC

FIGURE 17. Loss profile for Masirah network.

system load. The frequency deviation value is reduced by 24.7%, 9.3%, and 41.1% for 33 bus, 69 bus, and Masirah network, respectively, because the islanded microgrid has the ideal RDG size and placement together with active power allocation from VSG at the appropriate location. Moreover, power losses are reduced by 47.7%, 61.5%, and 39.1% for the three test systems. Moreover, as per the results, the VSGs provide 8.41, 8.76, and 9.43 MJ/MVA inertia to the grid for the 33 bus, 69 bus, and Masirah systems, respectively. The frequency deviation and total loss comparisons show that only

TABLE 5. MOSSA results for Masirah Island in 72 hour optimization period.

Parameter	Results
PV size (MVA)	2.71
WT size (MVA)	2.88
VSG size (MW)	5.78
PV location	49
WT location	35
VSG location	11
Frequency deviation (p.u)	0.000025
ROCOF(Hz/s)	0.2696
H (MJ/MVA)	9.351
TAES	51590.21
Power Losses (MWh)	7.08

TABLE 6. MOSSA results for only VSG placement.

Parameters	33 bus	69 bus	Masirah island
VSG size	2.2	2.16	5.67
VSG position	7	61	10
Power losses (kW)	105.83	84.75	183.43
ROCOF(Hz/s)	0.0185	0.0190	0.0539
H (MJ/MVA)	8.41	8.76	9.43
TAES (USD)	42337.7	59360.8	49848.8
Frequency deviation (p.u)	0.0702	0.0756	0.2382

TABLE 7. MOSSA results for only RDG placement.

Parameters	33 bus	69 bus	Masirah island
PV size	1.11	1.4	2.63
PV position	13	68	17
WT size	1.5	1.44	2.40
WT position	32	61	51
Power losses (kW)	59.91	84.19	159.72
ROCOF(Hz/s)	0.0182	0.0188	.0531
TAES (USD)	69330.7	81574.4	80840.6
Frequency deviation (p.u)	0.000647	0.000663	0.1891

VSG placement is inferior as a solution to simultaneous RDG and VSG placement scenarios since the low inertia problem is not completely alleviated.

C. ONLY RDG PLACEMENT

Table 7 displays the MOSSA results for only RDG placement. In this instance, the utility and the RDGs provide the system load, with the utility source linked to the grid. According to the results, the frequency deviation value is reduced by 99.3%, 99.2%, and 53.2% for the 33 bus, 69 bus, and the Masirah network, respectively, because the islanded microgrid has the ideal RDG size and placement together with active power allocation from VSG at the appropriate location. Moreover, power losses are reduced by 70.4%, 61.7%, and 46.9%, respectively. Due to the system's increased flexibility, two RDG units appear to perform better than the single VSG deployment scenario. Only RDG placement is inferior as a solution to simultaneous RDG and VSG placement scenarios, according to frequency deviation and total loss comparisons.

D. ROCOF ANALYSIS

Fig. 18 demonstrates the ROCOF analysis for the IEEE 33 bus, 69 bus, and Masirah Island network, respectively. The

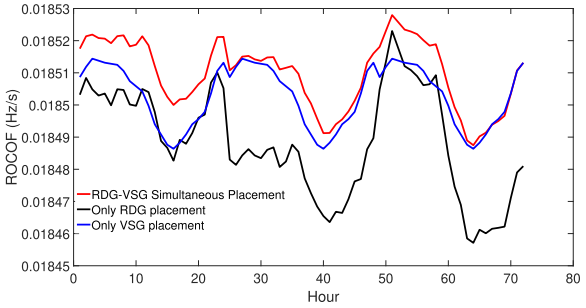

(a) IEEE 33 bus

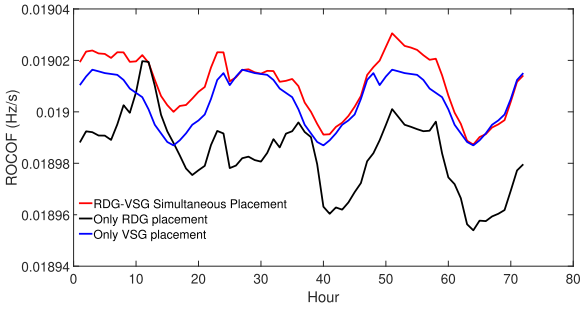

(b) IEEE 69 bus

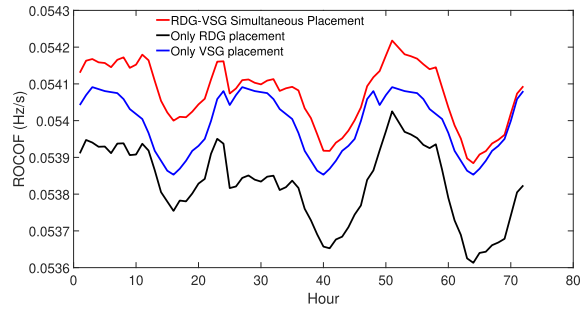

(c) Masirah Island

FIGURE 18. ROCOF analysis.

graph depicts the test systems' hourly average ROCOF values. The results show that the ROCOF values for only RDG placement instances are significantly higher due to the lack of inertia support. Besides, in the cases of only VSG placement and simultaneous VSG and RDG deployment, coupled active power allocation and inertia support from VSGs reduce the ROCOF value and so constitute an improved stable system.

E. RESULTS COMPARISON

As the searching performances of multi-objective algorithms are more sophisticated than those of single-objective algorithms, the results of each approach are compared using a *S*-index and a *C* metric [41], [47]. The definitions for these metrics are provided in the subsections that follow.

1) *S*-INDEX

The neighboring residual fitness function values alleviate the selection of evenly distributed Pareto solution sets. The NDS

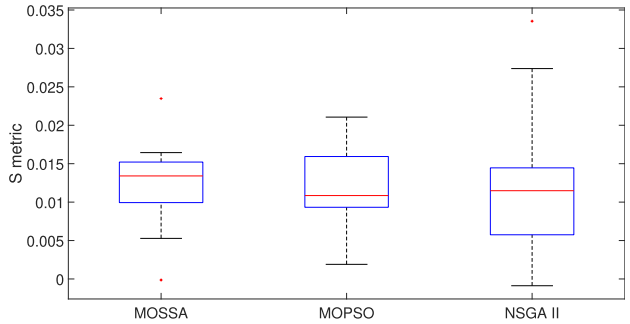

FIGURE 19. Spacing metrics for MOSSA, MOPSO and NSGA-II algorithms.

TABLE 8. *C* value results.

C	Average	Standard deviation	Maximum	Minimum
C (MOSSA,MOPSO)	12.7	17.7	38	2.1
C (MOSSA,NSGA II)	8.9	11.4	21	0

can be formulated as Eq. 20:

$$H_t = minimum[\sum_{p=1}^{t} S_{pYt} - S_{pYty}] \quad and\ ty = 1, 2, \ldots..q : q \neq 1 \tag{20}$$

This normalized minimum distance may be used with the spacing metric Eq. V-E1:

$$S = \sqrt{\frac{1}{tk}\sum_{t=1}^{q}(H_{ti} - H_t)^2} \tag{21}$$

As a result, the normal Euclidean distance is mathematically described by the following Eq. 22.

$$H_{ti} = \frac{1}{tk}\sum_{t=1}^{q}(H_{ti}) \tag{22}$$

Low S values indicate that Pareto solutions are evenly distributed, indicating superior solutions for specific concerns. The boxplot median in Fig. 19 can be used to measure the effectiveness of an algorithm. MOSSA is superior as it offers the smallest value with a constrained interval.

2) C

Consider the two PSCs O_1 and O_2 generated by the two different methods. The expression $O_{1,2}$ can be expressed as:

$$C(O_1, O_2) = \frac{|o_1 \varepsilon O_1; o_2 \varepsilon O_2 : o_1 \geq o_2| \times 100}{|O_2|} \tag{23}$$

Table 8 shows the C values for the abovementioned methods. The top row of the C index data shows that, on average, 87.3% of the results found by MOSSA outnumber those identified by MOPSO. Similar findings for the other rows demonstrate that MOSSA solutions perform better than MOPSO and NSGA-II solutions in terms of C index performance. Consequently, the C and S metric results show that MOSSA produces better Pareto front solutions than other methods.

VI. CONCLUSION

A unique MOSSA approach for simultaneous RDG and VSG size and placement in distribution networks is provided to improve frequency stability and minimize yearly energy-saving expenses. To account for Oman's weather-related fluctuation in RDG output, the simulation duration was adjusted to 72 hours for three seasons. Based on the findings, the following conclusions have been drawn:

- The best Pareto fronts satisfied the frequency stability and cost minimization.
- The hourly power losses and total energy losses were greatly reduced during the optimization period.
- The proposed multi-objective optimization strategy, which used seasonal load variance and Oman's stochastic RDG output powers, successfully improved the voltage profile of the networks. Furthermore, all of the Pareto front solutions avoided system voltage violations.
- Two performance measures were used to evaluate PSC sets of the MOSSA method with two multi-objective benchmark algorithms, notably the MOPSO and NSGA-II algorithms. The comparisons showed that the Pareto solutions generated by the MOSSA algorithm were more robust than those generated by the other two methods.

According to the results, this study can offer recommendations for improving the operating efficiency of current RDG-VSG integrated microgrid systems. The effects of installing renewable distributed generation with VSG on realistic networks might be explored in future studies. Furthermore, future development might involve techno-economic analysis and energy storage technologies combined with VSG and RDG units. The suggested system may also deal with real-time operational circumstances, provided the load and RDG output estimation is integrated.

REFERENCES

[1] A. P. Jha, A. Mahajan, S. K. Singh, and P. Kumar, "Renewable energy proliferation for sustainable development: Role of cross-border electricity trade," *Renew. Energy*, vol. 201, pp. 1189–1199, Dec. 2022, doi: 10.1016/j.renene.2022.11.046.

[2] Y. Shang, D. Han, G. Gozgor, M. K. Mahalik, and B. K. Sahoo, "The impact of climate policy uncertainty on renewable and non-renewable energy demand in the United States," *Renew. Energy*, vol. 197, pp. 654–667, Sep. 2022, doi: 10.1016/j.renene.2022.07.159.

[3] C. Pradhan, C. N. Bhende, and A. K. Samanta, "Adaptive virtual inertia-based frequency regulation in wind power systems," *Renew. Energy*, vol. 115, pp. 558–574, Jan. 2018, doi: 10.1016/j.renene.2017.08.065. [Online]. Available: https://www.sciencedirect.com/science/article/pii/S0960148117308236

[4] F. Ahmed, D. Al Kez, S. McLoone, R. J. Best, C. Cameron, and A. Foley, "Dynamic grid stability in low carbon power systems with minimum inertia," *Renew. Energy*, vol. 210, pp. 486–506, Jul. 2023, doi: 10.1016/j.renene.2023.03.082.

[5] C. Zhong, H. Li, Y. Zhou, Y. Lv, J. Chen, and Y. Li, "Virtual synchronous generator of PV generation without energy storage for frequency support in autonomous microgrid," *Int. J. Electr. Power Energy Syst.*, vol. 134, Jan. 2022, Art. no. 107343, doi: 10.1016/j.ijepes.2021.107343.

[6] M. Chen, D. Zhou, and F. Blaabjerg, "Active power oscillation damping based on acceleration control in paralleled virtual synchronous generators system," *IEEE Trans. Power Electron.*, vol. 36, no. 8, pp. 9501–9510, Aug. 2021, doi: 10.1109/TPEL.2021.3051272.

[7] M. Bakeer, G. Magdy, A. Bakeer, and M. M. Aly, "Resilient virtual synchronous generator approach using DC-link capacitor energy for frequency support of interconnected renewable power systems," *J. Energy Storage*, vol. 65, Aug. 2023, Art. no. 107230, doi: 10.1016/j.est.2023.107230.

[8] A. Engler and N. Soultanis, "Droop control in LV-grids," in *Proc. Int. Conf. Future Power Syst.*, Nov. 2005, p. 6, doi: 10.1109/FPS.2005.204224.

[9] J. Driesen and K. Visscher, "Virtual synchronous generators," in *Proc. IEEE Power Energy Soc. Gen. Meeting Convers. Del. Electr. Energy 21st Century*, Jul. 2008, pp. 1–3, doi: 10.1109/PES.2008.4596800.

[10] M. Shadoul, R. Ahshan, R. S. Alabri, A. Al-Badi, M. Albadi, and M. Jamil, "A comprehensive review on a virtual-synchronous generator: Topologies, control orders and techniques, energy storages, and applications," *Energies*, vol. 15, no. 22, p. 8406, Nov. 2022, doi: 10.3390/en15228406.

[11] P. Sun, J. Yao, Y. Zhao, X. Fang, and J. Cao, "Stability assessment and damping optimization control of multiple grid-connected virtual synchronous generators," *IEEE Trans. Energy Convers.*, vol. 36, no. 4, pp. 3555–3567, Dec. 2021, doi: 10.1109/TEC.2021.3104348.

[12] V. Thomas, S. Kumaravel, and S. Ashok, "Fuzzy controller-based self-adaptive virtual synchronous machine for microgrid application," *IEEE Trans. Energy Convers.*, vol. 36, no. 3, pp. 2427–2437, Sep. 2021, doi: 10.1109/TEC.2021.3057487.

[13] M. M. Mohamed, H. M. El Zoghby, S. M. Sharaf, and M. A. Mosa, "Optimal virtual synchronous generator control of battery/supercapacitor hybrid energy storage system for frequency response enhancement of photovoltaic/diesel microgrid," *J. Energy Storage*, vol. 51, Jul. 2022, Art. no. 104317, doi: 10.1016/j.est.2022.104317.

[14] A. Komijani, M. Sedighizadeh, and M. Kheradmandi, "Improving fault ride-through in meshed microgrids with wind and PV by virtual synchronous generator with SFCL and SMES," *J. Energy Storage*, vol. 50, Jun. 2022, Art. no. 103952, doi: 10.1016/j.est.2021.103952.

[15] M. Nour, G. Magdy, J. P. Chaves-Ávila, Á. Sánchez-Miralles, and F. Jurado, "A new two-stage controller design for frequency regulation of low-inertia power system with virtual synchronous generator," *J. Energy Storage*, vol. 62, Jun. 2023, Art. no. 106952, doi: 10.1016/j.est.2023.106952.

[16] A. Saleh, W. A. Omran, H. M. Hasanien, M. Tostado-Véliz, A. Alkuhayli, and F. Jurado, "Manta ray foraging optimization for the virtual inertia control of islanded microgrids including renewable energy sources," *Sustainability*, vol. 14, no. 7, p. 4189, Apr. 2022, doi: 10.3390/su14074189.

[17] A. Faragalla, O. Abdel-Rahim, M. Orabi, and E. H. Abdelhameed, "Enhanced virtual inertia control for microgrids with high-penetration renewables based on whale optimization," *Energies*, vol. 15, no. 23, p. 9254, Dec. 2022, doi: 10.3390/en15239254.

[18] R. K. Khadanga, D. Das, A. Kumar, and S. Panda, "Sine augmented scaled arithmetic optimization algorithm for frequency regulation of a virtual inertia control based microgrid," *ISA Trans.*, vol. 138, pp. 534–545, Jul. 2023, doi: 10.1016/j.isatra.2023.02.025.

[19] T. Santhoshkumar and V. Senthilkumar, "Transient and small signal stability improvement in microgrid using AWOALO with virtual synchronous generator control scheme," *ISA Trans.*, vol. 104, pp. 233–244, Sep. 2020, doi: 10.1016/j.isatra.2020.05.006.

[20] H. Yin, H. Lan, D. C. Yu, Y.-Y. Hong, and R.-Y. Li, "An improved optimal allocation scheme of energy storage system in a distribution system based on transient stability," *J. Energy Storage*, vol. 34, Feb. 2021, Art. no. 101977, doi: 10.1016/j.est.2020.101977.

[21] H. Nazaripouya, Y. Wang, P. Chu, H. R. Pota, and R. Gadh, "Optimal sizing and placement of battery energy storage in distribution system based on solar size for voltage regulation," in *Proc. IEEE Power Energy Soc. Gen. Meeting*, Jul. 2015, pp. 1–5, doi: 10.1109/pesgm.2015.7286059.

[22] M. B. Horasan and H. S. Kilic, "A multi-objective decision-making model for renewable energy planning: The case of Turkey," *Renew. Energy*, vol. 193, pp. 484–504, Jun. 2022, doi: 10.1016/j.renene.2022.04.158.

[23] A. Naderipour, S. A. Nowdeh, P. B. Saftjani, Z. Abdul-Malek, M. W. B. Mustafa, H. Kamyab, and I. F. Davoudkhani, "Deterministic and probabilistic multi-objective placement and sizing of wind renewable energy sources using improved spotted hyena optimizer," *J. Cleaner Prod.*, vol. 286, Mar. 2021, Art. no. 124941, doi: 10.1016/j.jclepro.2020.124941.

[24] A. Fathy, "A novel artificial hummingbird algorithm for integrating renewable based biomass distributed generators in radial distribution systems," *Appl. Energy*, vol. 323, Oct. 2022, Art. no. 119605, doi: 10.1016/j.apenergy.2022.119605.

[25] T. P. Nguyen, T. A. Nguyen, T. V.-H. Phan, and D. N. Vo, "A comprehensive analysis for multi-objective distributed generations and capacitor banks placement in radial distribution networks using hybrid neural network algorithm," *Knowl.-Based Syst.*, vol. 231, Nov. 2021, Art. no. 107387, doi: 10.1016/j.knosys.2021.107387.

[26] T. Gu, P. Wang, F. Liang, G. Xie, L. Guo, X.-P. Zhang, and F. Shi, "Placement and capacity selection of battery energy storage system in the distributed generation integrated distribution network based on improved NSGA-II optimization," *J. Energy Storage*, vol. 52, Aug. 2022, Art. no. 104716, doi: 10.1016/j.est.2022.104716.

[27] A. A. A. El-Ela, R. A. El-Sehiemy, A. M. Shaheen, W. A. Wahbi, and M. T. Mouwafi, "A multi-objective equilibrium optimization for optimal allocation of batteries in distribution systems with lifetime maximization," *J. Energy Storage*, vol. 55, Nov. 2022, Art. no. 105795, doi: 10.1016/j.est.2022.105795.

[28] K. Kasturi, C. K. Nayak, S. Patnaik, and M. R. Nayak, "Strategic integration of photovoltaic, battery energy storage and switchable capacitor for multi-objective optimization of low voltage electricity grid: Assessing grid benefits," *Renew. Energy Focus*, vol. 41, pp. 104–117, Jun. 2022, doi: 10.1016/j.ref.2022.02.006.

[29] K. Balu and V. Mukherjee, "Optimal allocation of electric vehicle charging stations and renewable distributed generation with battery energy storage in radial distribution system considering time sequence characteristics of generation and load demand," *J. Energy Storage*, vol. 59, Mar. 2023, Art. no. 106533, doi: 10.1016/j.est.2022.106533.

[30] T. Weckesser, D. F. Dominković, E. M. V. Blomgren, A. Schledorn, and H. Madsen, "Renewable energy communities: Optimal sizing and distribution grid impact of photo-voltaics and battery storage," *Appl. Energy*, vol. 301, Nov. 2021, Art. no. 117408, doi: 10.1016/j.apenergy.2021.117408.

[31] S. Mishra, G. Saini, A. Chauhan, S. Upadhyay, and D. Balakrishnan, "Optimal sizing and assessment of grid-tied hybrid renewable energy system for electrification of rural site," *Renew. Energy Focus*, vol. 44, pp. 259–276, Mar. 2023, doi: 10.1016/j.ref.2022.12.009.

[32] E. Grover-Silva, R. Girard, and G. Kariniotakis, "Optimal sizing and placement of distribution grid connected battery systems through an SOCP optimal power flow algorithm," *Appl. Energy*, vol. 219, pp. 385–393, Jun. 2018, doi: 10.1016/j.apenergy.2017.09.008.

[33] Y. Li, B. Feng, B. Wang, and S. Sun, "Joint planning of distributed generations and energy storage in active distribution networks: A bi-level programming approach," *Energy*, vol. 245, Apr. 2022, Art. no. 123226, doi: 10.1016/j.energy.2022.123226.

[34] B. Ahmadi, O. Ceylan, A. Ozdemir, and M. Fotuhi-Firuzabad, "A multi-objective framework for distributed energy resources planning and storage management," *Appl. Energy*, vol. 314, May 2022, Art. no. 118887, doi: 10.1016/j.apenergy.2022.118887.

[35] N. Khalesi, N. Rezaei, and M.-R. Haghifam, "DG allocation with application of dynamic programming for loss reduction and reliability improvement," *Int. J. Electr. Power Energy Syst.*, vol. 33, no. 2, pp. 288–295, Feb. 2011, doi: 10.1016/j.ijepes.2010.08.024.

[36] s. Alnaser and L. F. Ochoa, "Optimal sizing and control of energy storage in wind power-rich distribution networks," in *Proc. IEEE Power Energy Soc. Gen. Meeting (PESGM)*, Jul. 2016, p. 1, doi: 10.1109/pesgm.2016.7741202.

[37] N. Ntube and H. Li, "Stochastic multi-objective optimal sizing of battery energy storage system for a residential home," *J. Energy Storage*, vol. 59, Mar. 2023, Art. no. 106403, doi: 10.1016/j.est.2022.106403.

[38] R. Al Afif, Y. Ayed, and O. N. Maaitah, "Feasibility and optimal sizing analysis of hybrid renewable energy systems: A case study of al-karak, Jordan," *Renew. Energy*, vol. 204, pp. 229–249, Mar. 2023, doi: 10.1016/j.renene.2022.12.109.

[39] H. M. Ridha, C. Gomes, H. Hizam, and S. Mirjalili, "Multiple scenarios multi-objective Salp swarm optimization for sizing of standalone photovoltaic system," *Renew. Energy*, vol. 153, pp. 1330–1345, Jun. 2020, doi: 10.1016/j.renene.2020.02.016.

[40] M. S. Abid, H. J. Apon, K. A. Morshed, and A. Ahmed, "Optimal planning of multiple renewable energy-integrated distribution system with uncertainties using artificial hummingbird algorithm," *IEEE Access*, vol. 10, pp. 40716–40730, 2022, doi: 10.1109/ACCESS.2022.3167395.

[41] B. Ahmadi, O. Ceylan, and A. Ozdemir, "A multi-objective optimization evaluation framework for integration of distributed energy resources," *J. Energy Storage*, vol. 41, Sep. 2021, Art. no. 103005, doi: 10.1016/j.est.2021.103005.

[42] A. Bostan, M. S. Nazar, M. Shafie-khah, and J. P. S. Catalão, "Optimal scheduling of distribution systems considering multiple downward energy hubs and demand response programs," *Energy*, vol. 190, Jan. 2020, Art. no. 116349, doi: 10.1016/j.energy.2019.116349.
[43] J.-N. Sheen, M.-T. Tsai, and S.-W. Wu, "A benefits analysis for wind turbine allocation in a power distribution system," *Energy Convers. Manage.*, vol. 68, pp. 305–312, Apr. 2013, doi: 10.1016/j.enconman.2012.12.022.
[44] H. A. Kazem, H. A. S. Al-Badi, A. S. Al Busaidi, and M. T. Chaichan, "Optimum design and evaluation of hybrid solar/wind/diesel power system for Masirah Island," *Environ., Develop. Sustainability*, vol. 19, no. 5, pp. 1761–1778, Oct. 2017, doi: 10.1007/s10668-016-9828-1.
[45] S. A. Abdul-Wahab, Y. Charabi, A. M. Al-Mahruqi, and I. Osman, "Design and evaluation of a hybrid energy system for Masirah Island in Oman," *Int. J. Sustain. Eng.*, vol. 13, no. 4, pp. 288–297, Jul. 2020, doi: 10.1080/19397038.2020.1790057.
[46] F. B. Ismail, M. N. Mahdi, A. A. Salah, N. F. O. Al-Muhsen, M. M. Shalby, and Y. K. Al Nafie, "Feasibility study of wind energy generation systems in Masirah island: Real case study," in *Proc. Int. Conf. Electr. Eng. Informat. (ICEEI)*, Oct. 2021, pp. 1–6, doi: 10.1109/ICEEI52609.2021.9611138.
[47] K.-Y. Liu, W. Sheng, Y. Liu, X. Meng, and Y. Liu, "Optimal sitting and sizing of DGs in distribution system considering time sequence characteristics of loads and DGs," *Int. J. Electr. Power Energy Syst.*, vol. 69, pp. 430–440, Jul. 2015, doi: 10.1016/j.ijepes.2015.01.033.

MD. SHADMAN ABID (Student Member, IEEE) received the B.Sc. degree in electrical and electronic engineering (EEE) from the Islamic University of Technology (IUT), Gazipur, Bangladesh, in 2022. He is currently a Research Assistant with the Department of Electrical and Computer Engineering, Sultan Qaboos University (SQU), Muscat, Oman, under the "System Inertia Enhanced-Based Control System Development for Microgrid Application" Project. His research interests include control system development, power system optimization, power quality, electric vehicles, distributed generation, distribution automation, and microgrids.

RAZZAQUL AHSHAN (Senior Member, IEEE) received the B.Sc. degree in electrical and computer engineering from the Khulna University of Engineering & Technology, Bangladesh, in 2002, and the M.Eng. and Ph.D. degrees in electrical engineering from the Memorial University of Newfoundland, St. John's, NL, Canada, in 2008 and 2013, respectively, with a scholarship from the Natural Sciences and Engineering Research Council of Canada (NSERC). He was a Lecturer for three years with the Khulna University of Engineering & Technology. In 2011, he joined the College of North Atlantic, Newfoundland, Canada, as a Faculty Member and a Researcher, until August 2016. Currently, he is an Associate Professor with the Department of Electrical and Computer Engineering, Sultan Qaboos University (SQU), Muscat, Oman. His research interests include electrical machines and drives, power electronic converters, renewable energy systems, microgrids, smart grids, energy management and control, energy storage, green hydrogen, system reliability modeling, and digital signal processing techniques and their applications in power systems. He was a recipient of the Distinguished Academician Award, in 2021, Sultan Qaboos University, Oman; Best Paper Award, in 2021, and IEEE Oman Section. He is a fellow of the School of Graduate Studies, in 2013, Memorial University of Newfoundland, Canada; and the Prime Minister Gold Medal Award, in 2002, Khulna University of Engineering & Technology.

RASHID AL-ABRI (Member, IEEE) received the B.Sc. degree in electrical engineering from Sultan Qaboos University (SQU), Oman, in 2002, the M.Sc. degree in electrical engineering from the Curtin University of Technology, Western Australia, in 2004, and the Ph.D. degree from the Department of Electrical and Computer Engineering, University of Waterloo, Waterloo, ON, Canada, in 2012. Currently, he is an Associate Professor with the ECE Department, SQU, where he is also the Director of the Sustainable Energy Research Center (SERC). His research interests include power electronics applications, renewable energy, power quality, energy efficiency, power systems, smart grid applications, and power system stability. In addition, he is also leading some research on the areas of green hydrogen, carbon capture, use and storage (CCUS), and net zero emissions.

ABDULLAH AL-BADI (Senior Member, IEEE) received the M.Sc. and Ph.D. degrees from UMIST, U.K., in 1993 and 1998, respectively. He has published more than 200 publications and co-author one edited book. He carried out 46 research projects and consultancy (main or co-investigator), with total attracted fund of + USD 2.2 million. He is among the Stanford University's world's top 2% scientists, in 2021. He is a Consultant with the Oman Society of Engineers. He is the Chair for IEEE Oman Section. He is an IEEE Program Evaluator of Accreditation Board for Engineering and Technology (ABET) and an External Reviewer of Oman Academic Accreditation Authority (OAAA). In 2009, he was appointed as the Dean of the Deanship of Admissions and Registration. In February 2014, he was appointed as the Dean of the College of Engineering. Currently, he is the Research Chair, Madayn for the Development of Industrial Estates and Free Zones, and a Professor with the Electrical and Computer Engineering Department, Sultan Qaboos University.

MOHAMMED ALBADI (Senior Member, IEEE) received the B.Sc. degree in electrical and electronics engineering from Sultan Qaboos University (SQU), Oman, in 2000, the M.Sc. degree in electrical engineering from the Aachen University of Technology (RWTH-Aachen), Germany, in 2003, and the Ph.D. degree in electrical and computer engineering from the University of Waterloo (UWaterloo), Canada, in 2010. He is currently the Rector with Arab Open University Oman. Previously, he was a Professor and the Head of Electrical and Computer Engineering with SQU, a Visiting Associate Professor with UWaterloo, and an Engineer with Petroleum Development Oman. His research interests include renewable energy, distributed generation, power quality, demand-side management, power system operation and planning, and power system economics. In these fields, he published over 100 peer-reviewed international journal articles and conference papers and conducted numerous industry-funded research projects. He was a recipient of several awards, including the SQU Best Researcher Award, SQU Research Excellence Award, and Best Paper Award in the *International Journal of Electrical and Electronics Engineering*, in 2019. He was listed among the top 2% of the Stanford University's world's most highly-cited scholars for the years 2019, 2020, and 2021. He is a member of the Oman Society of Engineers. He served as an Associate Editor for the *International Journal of Electrical and Education* (IJEEE) and the *Journal of Engineering Research* (TJER) and a reviewer for numerous peer-reviewed journals and conferences.